




# Growth and characterization of organic 2,2',4,4'-tetrahydroxybenzophenone single crystals for nonlinear optical applications

M. L. Lima Rose<sup>1,2</sup>, T. Suthan<sup>3,\*</sup> , S. Goma<sup>3</sup>, C. Gnanasambandam<sup>1</sup>, and T. C. Sabari Girisun<sup>4</sup>

<sup>1</sup>Department of Physics & Research Centre, S.T. Hindu College, Nagercoil 629002, India

<sup>2</sup>Department of Physics, Malankara Catholic College, Mariagiri 629153, India

<sup>3</sup>Department of Physics, Lekshmipuram College of Arts and Science, Neyyoor, Tamil Nadu 629802, India

<sup>4</sup>Nanophotonics Laboratory, School of Physics, Bharathidasan University, Tiruchirappalli 620024, India

Received: 13 May 2023

Accepted: 18 July 2023

Published online:

17 August 2023

© The Author(s), under exclusive licence to Springer Science+Business Media, LLC, part of Springer Nature 2023

## ABSTRACT

The organic 2,2',4,4'-tetrahydroxybenzophenone single crystal was grown by slow evaporation solution growth technique. The single crystal X-ray diffraction studies show that the grown 2,2',4,4'-tetrahydroxybenzophenone crystal belongs to the monoclinic crystal system with the centrosymmetric space group of C2/c. The grown crystals' functional groups have been identified by the FTIR and FT-Raman spectral studies. The UV-Visible studies show that the cut-off wavelength was observed around 401 nm and the grown crystal has good transmittance in the visible regions. The optical parameters such as optical band gap ( $E_g$ ), extinction coefficient ( $K$ ), Urbach energy ( $E_U$ ), and skin depth ( $\delta$ ) were calculated. The TG/DTA analyses were used to find the thermal stability of the grown crystal. The dielectric properties of the grown 2,2',4,4'-tetrahydroxybenzophenone single crystal were analyzed by using the parallel plate capacitor method. The nonlinear optical properties of the grown 2,2',4,4'-tetrahydroxybenzophenone crystal was measured using the Z-scan technique. The grown 2,2',4,4'-tetrahydroxybenzophenone single crystals optical limiting threshold values were analyzed.

## 1 Introduction

Nowadays, optoelectronics is a developing field that uses the unique properties of organic materials to increase new applications due to their low cost, lightweight, and processing ability [1]. The

microelectronics industries are persistently endeavouring to revive themselves to identify new technical solutions to keep up with the drift of expanding gadget strength in ultra-large scale integrated (ULSI) circuits. The new low dielectric constant ( $\epsilon_r$ ) materials are widely used in multi-level interconnects. The

Address correspondence to E-mail: suthantr@yahoo.co.in

interconnect networks are surrounded and insulated using interlayer dielectrics. Lowering the interlayer dielectric (ILD) value reduces the RC delay, power consumption, and crosstalk between nearby interconnects [2–5]. The materials have good biological properties are used for medical applications [6–8]. Organic Nonlinear Optical (NLO) materials play a crucial role in the frequency conversion of high-power lasers, optical data storage, and high-speed optical communication systems [9]. Organic NLO crystals have more significant advantages than inorganic equivalents because of their wide range of transparency. The defect-free organic NLO single crystals are helpful in frequency-tunable laser radiation for photonics in the ultraviolet, blue, and green wavelength regions [10]. Many organic benzophenone derivative single crystals have good nonlinear optical properties. The various benzophenone derivative single crystals were grown in numerous ways, and their structural and optical properties were studied [11]. The benzophenone derivatives are mainly used for UV screens to save industrial goods from light induce damage [5]. The benzophenone derivatives are also used in optoelectronics to act as a photoresist in microelectronic circuits. In 2,2',4,4'-tetrahydroxybenzophenone has two symmetry-independent molecules with strong intramolecular hydrogen bonds between the keto O atom and ortho hydroxyl groups. The O...O distances of intramolecular hydrogen bonds are varied due to the changes in crystallographic nature (intermolecular hydrogen bonding). All hydroxyl group acts as a donor to an intramolecular or intermolecular hydrogen bond to another hydroxyl O atom or a carbonyl O atom. The hydroxyl groups present in ortho with the largest intramolecular O...O distance is the donor for the bifurcated hydrogen bond [12]. The 2,2',4,4'-tetrahydroxybenzophenone was called Uvinul D50. It was figured out to do as a weak competitive inhibitor. It was found in products like soaps, shampoos, cosmetics, and sunscreen agents [13]. In the present study, 2,2',4,4'-tetrahydroxybenzophenone single crystals were grown by the slow evaporation solution growth method. The grown crystal was analyzed by single crystal XRD, FTIR, FT-Raman, UV-Vis, TG/DTA, dielectric, and NLO studies.

## 2 Experimental

The organic material 2,2',4,4'-tetrahydroxybenzophenone was purchased from Sigma Aldrich. The material was not soluble in water. Ethanol was found as an excellent solvent for growing 2,2',4,4'-tetrahydroxybenzophenone single crystals. The solubility was analyzed by the gravimetric method using various temperatures from 30 to 50 °C. The solubility graph is shown in Fig. 1. For single crystal growth, the homogeneous mixture was prepared by dissolving 2,2',4,4'-tetrahydroxybenzophenone in ethanol solvent continuously for about 5 h using the magnetic stirrer. It was filtered by Whatman filter paper to separate the entire impurities. Then the container was closed with a perforated polythene sheet, and the mixture was kept to crystallize at normal room temperature. The transparent good quality 2,2',4,4'-tetrahydroxybenzophenone single crystal was harvested. The grown 2,2',4,4'-tetrahydroxybenzophenone single crystal is shown in Fig. 2.

## 3 Results and discussion

### 3.1 X-ray diffraction studies

The crystallographic parameters of the grown 2,2',4,4'-tetrahydroxybenzophenone single crystal were analyzed by using Enraf Nonius CAD4MV31 single crystal X-ray diffractometer with the MoK $\alpha$

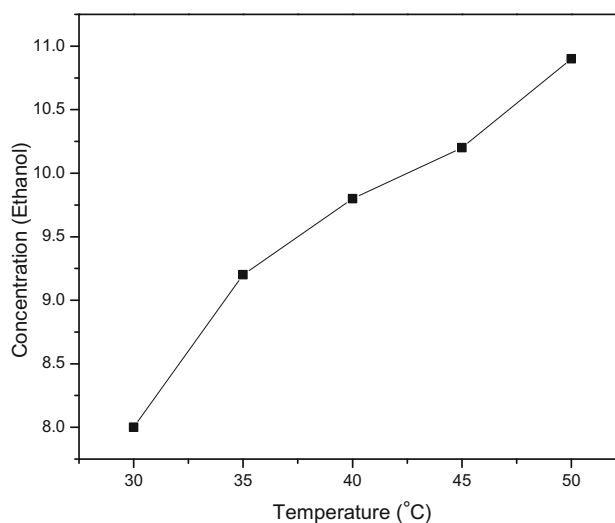


**Fig. 1** Solubility graph of 2,2',4,4'-tetrahydroxybenzophenone

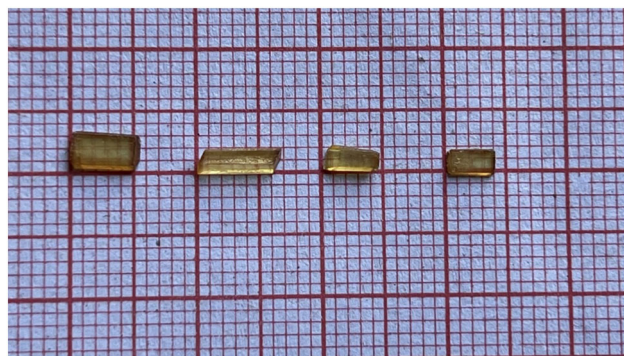


**Fig. 2** Photograph of 2,2',4,4'-tetrahydroxybenzophenone single crystals

radiation ( $\lambda = 0.71073 \text{ \AA}$ ). It is directly connected to the single crystal refinement module system, where the data was generated from X-ray analysis and is interpreted and refined to define the crystal structure. The crystal structure was found by the direct method of 15,663 reflections, and using the SHELXL97 package, the refinements were determined using the full-matrix least-squares technique. The results show that the grown 2,2',4,4'-tetrahydroxybenzophenone single crystal belongs to a monoclinic crystal system with the centrosymmetric space group C2/c. In this crystal structure, the molecule sits on the two-fold axis. The technical information, such as data acquisition, cell parameters, and selected processing results, are shown in Table 1. The molecular structure with crystallographic numbering scheme of the grown 2,2',4,4'-tetrahydroxybenzophenone single crystal is shown in Fig. 3a. Here the  $C_7=O_3$  carbonyl group resides on the symmetry element and the molecule sits on a twofold axis at  $(1/2, y, 1/4)$ . The grown crystal's packing diagram is shown in Fig. 3b.

### 3.2 FTIR and FT-Raman analyses

The grown crystal's functional groups were analyzed by using the FTIR and FT-Raman spectroscopic techniques. The grown 2,2',4,4'-tetrahydroxybenzophenone single crystal FTIR spectrum was analyzed by Perkin-Elmer FTIR spectrum RIX spectrometer with the KBr pellet technique, on a region of 4000 to 400  $\text{cm}^{-1}$ . The FT-Raman spectrum was recorded by BRUKER-RFS27: FT-Raman spectrometer in the region of 3500 to 50  $\text{cm}^{-1}$ . The recorded FTIR spectrum of the grown 2,2',4,4'-tetrahydroxybenzophenone is shown in Fig. 4. The FT-Raman spectrum of the grown 2,2',4,4'-

tetrahydroxybenzophenone is shown in Fig. 5. The peaks observed at 3507 and 3412  $\text{cm}^{-1}$  in the FTIR spectrum have been attributed to hydroxy group H-bonded OH stretching vibration. The peak observed at FTIR in 1600  $\text{cm}^{-1}$ , and the FT-Raman peak at 1628  $\text{cm}^{-1}$  were due to the C=C stretching vibrations. The peak observed at 1511  $\text{cm}^{-1}$  in the FTIR spectrum, and 1501  $\text{cm}^{-1}$  in FT-Raman are owing to C=C-C aromatic ring stretching vibrations. The FTIR peak observed at 1338  $\text{cm}^{-1}$  and the FT-Raman peak at 1378  $\text{cm}^{-1}$  reveal the O-H in plane bending vibration. The FTIR peaks observed at 1173  $\text{cm}^{-1}$ , 1133  $\text{cm}^{-1}$ , 978  $\text{cm}^{-1}$  and the FT-Raman peak observed at 1111  $\text{cm}^{-1}$  are due to C-H aromatic in plane bending vibrations. The peak observed at 634  $\text{cm}^{-1}$  in FTIR and 675  $\text{cm}^{-1}$  in FT-Raman are due to C-H bending vibration [14–18]. The observed peaks in both FTIR and FT-Raman spectra with their specified assignments are shown in Table 2.

### 3.3 UV-Vis studies

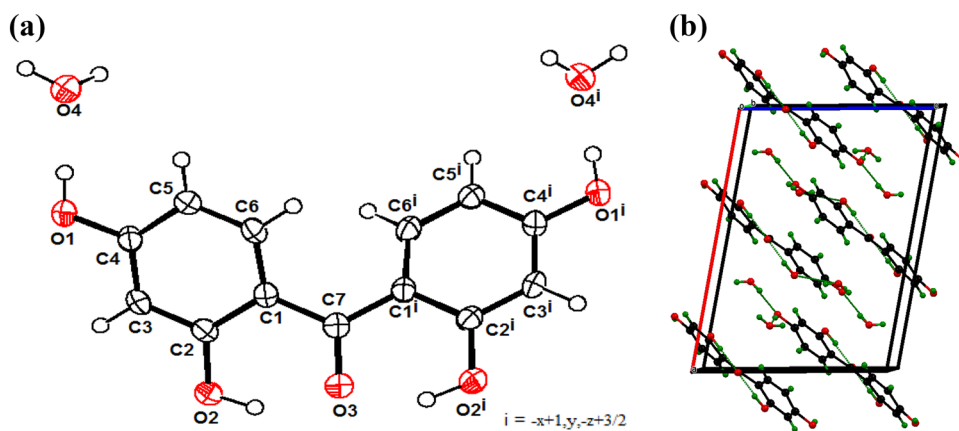
The organic benzophenone derivative single crystals have good optical properties. The grown organic 2,2',4,4'-tetrahydroxybenzophenone single crystal was analyzed by using Perkin-Elmer Lambda 35 UV spectrophotometer at the wavelength region 200 to 800 nm. The recorded transmittance spectrum is shown in Fig. 6a. The result reveals that the grown crystal's cut-off wavelength was observed around 401 nm and the crystal has good transmittance in the visible region. The grown 2,2',4,4'-tetrahydroxybenzophenone crystal may have potential applications in UV-tunable lasers. The electronic transition  $\sigma \rightarrow \sigma^*$  falls into the far-UV region,  $\pi \rightarrow \pi^*$ ,  $n \rightarrow \sigma^*$  transitions appear on the borderline of the near-UV and far-UV regions,  $n \rightarrow \pi^*$  transition falls into the near-UV and visible regions [19]. The grown 2,2',4,4'-tetrahydroxybenzophenone single crystal may have  $n \rightarrow \pi^*$  transition. The optical-absorption coefficient ( $\alpha$ ) can be estimated by the transmittance data using the relation [20, 21]

$$\alpha = \frac{2.3026 \log\left(\frac{1}{T}\right)}{t} \quad (1)$$

In the above relation,  $T$  denotes the transmittance and  $t$  denotes the thickness of the grown crystal. By plotting the Tauc plot as  $(\alpha h\nu)^2$  versus  $h\nu$  and extending the linear portion to the incident energy, the optical band gap was obtained. The experimental

**Table 1** 2,2',4,4'-tetrahydroxybenzophenone single crystal XRD data and structure refinement parameters

Empirical formula	$C_{13} H_{14} O_7$	
Formula weight	282.24	
Temperature	296(2) K	
Wavelength	0.71073 Å	
Crystal system	Monoclinic	
Space group	C2/c	
Unit cell dimensions	$a = 15.175(3)$ Å $b = 7.7791(15)$ Å $c = 11.087(2)$ Å	$\alpha = 90^\circ$ $\beta = 100.664(8)^\circ$ $\gamma = 90^\circ$
Volume	$1286.2(5)$ Å <sup>3</sup>	
Z	4	
Density (calculated)	$1.458$ Mg/m <sup>3</sup>	
Absorption coefficient	$0.120$ mm <sup>-1</sup>	
F (000)	592	
Crystal size	$0.284 \times 0.199 \times 0.038$ mm <sup>3</sup>	
Theta range for data collection	$3.358$ to $26.993^\circ$	
Index ranges	$-19 < = h < = 19, -9 < = k < = 9, -14 < = l < = 14$	
Reflections collected	15,663	
Independent reflections	1395 [ $R(\text{int}) = 0.0516$ ]	
Completeness to theta = $25.242^\circ$	99.7%	
Absorption correction	Semi-empirical from equivalents	
Max. and min. transmission	0.983 and 0.953	
Refinement method	Full-matrix least-squares on $F^2$	
Data/restraints/parameters	1395/0/108	
Goodness-of-fit on $F^2$	1.069	
Final R indices [ $I > 2\sigma(I)$ ]	$R1 = 0.0398, wR2 = 0.1093$	
R indices (all data)	$R1 = 0.0500, wR2 = 0.1172$	
Extinction coefficient	n/a	
Largest diff. peak and hole	$0.217$ and $-0.186$ e.Å <sup>-3</sup>	

**Fig. 3 a** Crystallographic numbering scheme of grown 2,2',4,4'-tetrahydroxybenzophenone single crystal. **b** Packing diagram of 2,2',4,4'-tetrahydroxybenzophenone single crystal

band gap value is 2.5 eV. It is shown in Fig. 6b. Due to this forbidden band gap, the grown crystal is suitable for photonic and optical applications [22, 23]. The amount of absorption produced by the

electromagnetic wave transmissions on the medium is defined by the term extinction coefficient ( $K$ ), which is connected to an absorption coefficient ( $\alpha$ ) and wavelength ( $\lambda$ ), by the relation [24–26]

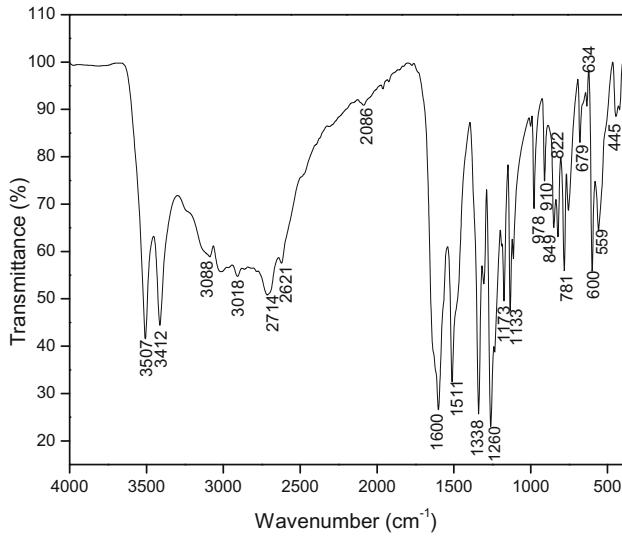


Fig. 4 FTIR spectrum of 2,2',4,4'-tetrahydroxybenzophenone

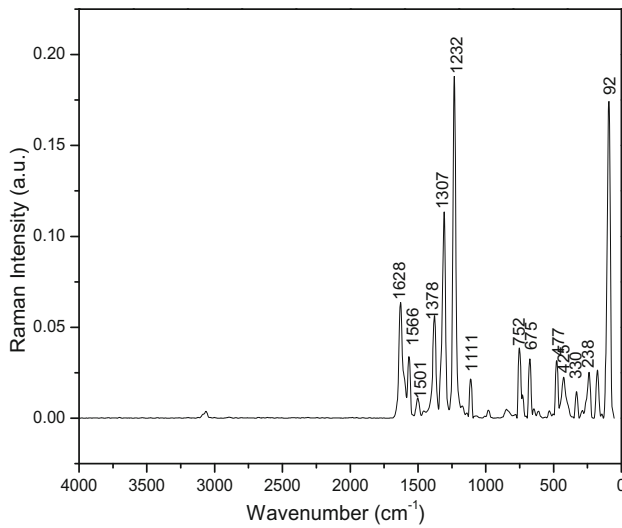


Fig. 5 FT-Raman spectrum of 2,2',4,4'-tetrahydroxybenzophenone

$$K = \frac{\lambda\alpha}{4\pi} \tag{2}$$

The plot drawn between the extinction coefficient and the wavelength is shown in Fig. 6c. The obtained extinction coefficient value is low, it may be due to the least absorption of incident radiation of the grown crystal. The Urbach energy ( $E_U$ ) is computed by the exponential formula [27, 28]

$$\alpha = \alpha_0 \exp\left(\frac{h\nu}{E_U}\right) \tag{3}$$

where  $E_U$  is the Urbach energy,  $\alpha_0$  is constant, and  $\alpha$  is the optical-absorption coefficient. Taking log on both sides of the above relation as

$$\ln(\alpha) = \ln(\alpha_0) + \frac{h\nu}{E_U} \tag{4}$$

The graph plot between  $\ln(\alpha)$  and the incident photon energy ( $h\nu$ ) is shown in Fig. 6d. The calculated Urbach energy value is 0.182 eV. It was obtained from the inverse slope. The result shows that the 2,2',4,4'-tetrahydroxybenzophenone single crystal has an good crystalline nature. The steepness parameter ( $\sigma$ ) can be calculated by using the relation [29].

$$\sigma = \left(\frac{k_B T}{E_U}\right) \tag{5}$$

The calculated steepness parameter value is 0.129. The electron-phonon interaction was calculated by using the formula [29]

$$E_{e-p} = \frac{2}{3\sigma} \tag{6}$$

The strength of the electron-phonon interaction ( $E_{e-p}$ ) is 5.1679. The skin depth ( $\delta$ ) depends on the amount of electromagnetic radiation penetrating the material. The skin depth was calculated by using the formula [30]

$$\delta = \frac{1}{\alpha} \tag{7}$$

The relation between skin depth and photon energy is shown in Fig. 6e. The result reveals that skin depth ( $\delta$ ) decreases with an increase in photon energy, which tells that the grown 2,2',4,4'-tetrahydroxybenzophenone single crystal is suitable for optoelectronic applications. The calculated optical parameter values are shown in Table 3.

### 3.4 Thermal analysis

The thermal properties of the grown 2,2',4,4'-tetrahydroxybenzophenone crystal were studied using Thermogravimetric (TG) and Differential Thermal Analyses (DTA). The TG and DTA techniques play a crucial role in investigating the thermal behaviour of grown crystals under a gradual increase in temperature. Thermogravimetry (TG) is defined as the

**Table 2** Molecular vibrational assignments of 2,2',4,4'-tetrahydroxybenzophenone

Wave number (cm <sup>-1</sup> ) reference range	FTIR (cm <sup>-1</sup> )	FT-Raman (cm <sup>-1</sup> )	Functional group	Assignment
3570–3200	3507 3412		Hydroxy group	Assignment
1615–1580	1600	1628	C=C	Stretching vibration
1510–1450	1511	1501	C=C–C	Aromatic ring stretching
1350–1260	1338	1378	O–H	In plane bending vibrations
1225–950	1173 1133 978	1111	C–H	Aromatic in plane bending vibration
810–750	781	752	Aromatic	1,3(Meta) disubstituted
680–610	634	675	C–H	bending

change in mass of a sample as a function of temperature when subjected to a controlled temperature. The observed TG/DTA graph is shown in Fig. 7a. In DTA, the peak observed around 208 °C is assigned as the melting point of the grown crystal. In DTA peak observed around 397 °C is attributed to the decomposition point of the grown crystal. The various non-isothermal methods are developed to determine the kinetic and thermodynamic parameters. The obtained TGA data can be used to study the kinetic parameters. Coats & Redfern (1997) developed a method to determine the kinetic parameters. The Coats & Redfern equation is [31–33].

$$\ln \left[ \frac{1 - (1 - \alpha)^{1-n}}{T^2(1-n)} \right] = \ln \left[ \left( \frac{AR}{\beta E_a} \right) \left( 1 - \frac{2RT}{E_a} \right) \right] - \frac{E_a}{RT} \text{ for } n \neq 1 \quad (8)$$

Fractional weight loss ( $\alpha$ ) can be calculated using the formula.

$$\alpha = \frac{W_0 - W}{W_0 - W_f} \quad (9)$$

In the above equation,  $W_0$  is the starting weight,  $W$  is the instantaneous weight, and  $W_f$  is the final weight of the thermal-deterioration process, respectively. Here  $n$  denote the order of reaction,  $T$  indicate the absolute temperature,  $A$  represents the frequency factor,  $R$  denotes the gas constant ( $R = 8.317 \text{ Jmol}^{-1} \text{ K}^{-1}$ ),  $\beta$  denotes the rate of heat per second, and  $E_a$  denotes the activation energy. The Coats & Redfern equation for the first-order reaction ( $n = 1$ ) is given by

$$\ln \left[ \frac{-\ln(1-\alpha)}{T^2} \right] = \ln \left[ \left( \frac{AR}{\beta E_a} \right) \left( 1 - \frac{2RT}{E_a} \right) \right] - \frac{E_a}{RT} \text{ for } n = 1 \quad (10)$$

By plotting the graph in-between  $\ln \left[ \frac{-\ln(1-\alpha)}{T^2} \right]$  and  $1000/T$  is shown in Fig. 7b. The results show a straight line, from the slope activation energy ( $E_a$ ) is calculated, and the point of intersection is used to calculate the frequency factor ( $A$ ). The thermodynamic parameters, such as enthalpy of activation ( $\Delta H^*$ ), the entropy of activation ( $\Delta S^*$ ), and Gibb's free energy ( $\Delta G^*$ ) were calculated by the equation.

$$\Delta H^* = E_a - RT_m \quad (11)$$

$$\Delta S^* = R \ln \left( \frac{Ah}{k_B T_m} \right) \quad (12)$$

where  $h$  = Planck's constant ( $6.626 \times 10^{-34} \text{ J s}$ ) and  $k_B$  denotes the Boltzmann constant

$$Z = \frac{k_B T_m}{h} \exp \left( \frac{\Delta S^*}{R} \right) \quad (13)$$

$$\Delta G^* = \Delta H^* - T_m \Delta S^* \quad (14)$$

The calculated kinetic and thermodynamic parameters are shown in Table. 4. The positive value of enthalpy indicates that the process was endothermic. The activation entropy has negative values, which shows that the decomposition reactions proceed with a lower rate than normal ones. The negative value of the entropy of activation indicates that the activated complex is more ordered than the reactant and the decomposition reaction is slow. It may be due to the chemisorption of oxygen and the

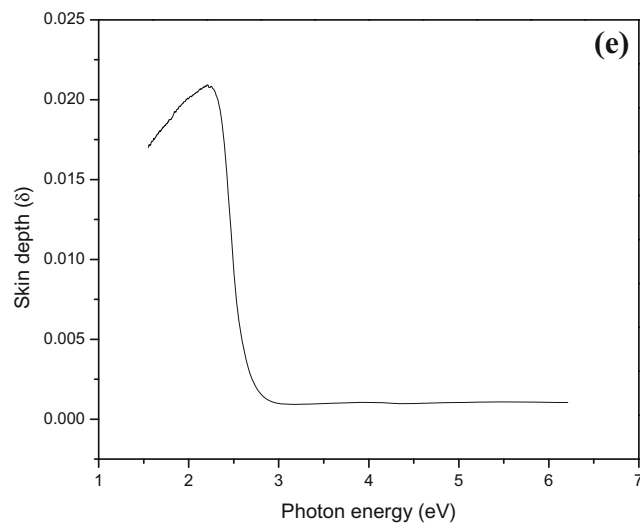
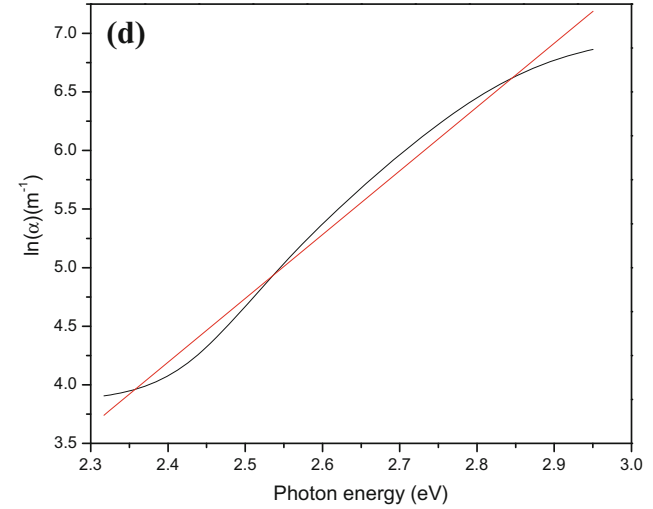
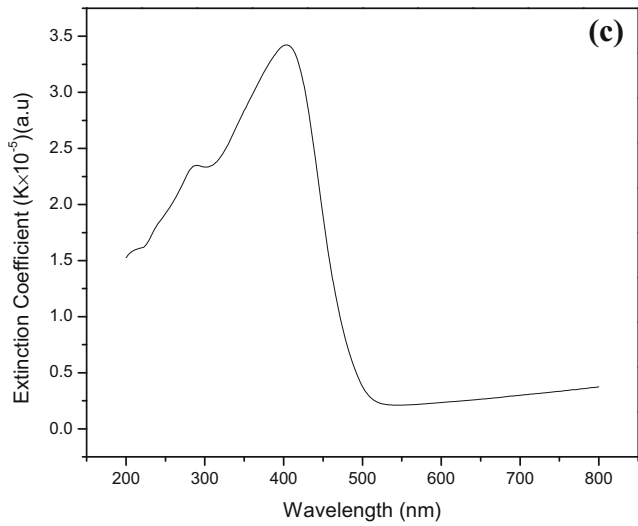
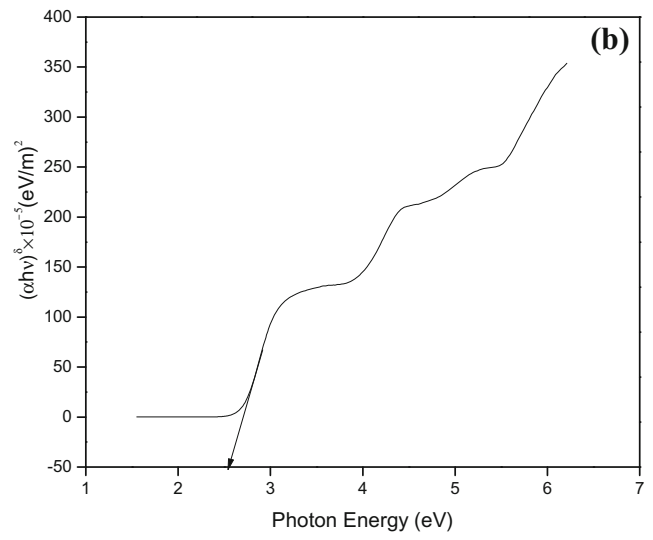
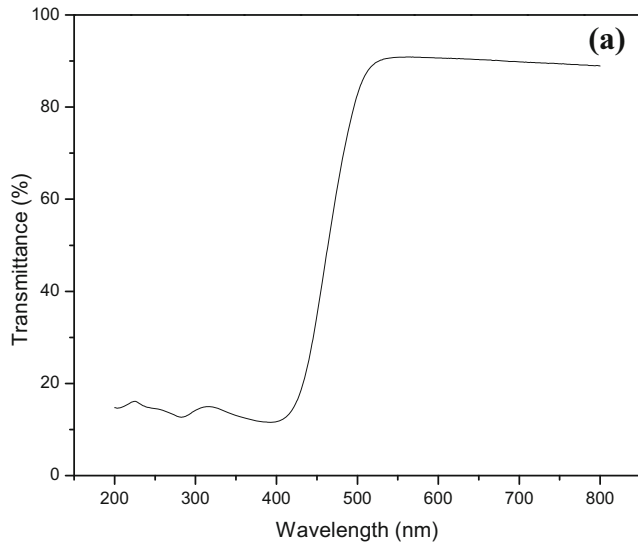


**Fig. 6** **a** UV–Vis transmission spectrum of 2,2',4,4'-tetrahydroxybenzophenone. **b** Tauc plot of  $(\alpha h\nu)^2$  versus Photon energy ( $h\nu$ ) of 2,2',4,4'-tetrahydroxybenzophenone. **c** Plot of extinction coefficient versus wavelength of grown 2,2',4,4'-tetrahydroxybenzophenone single crystal. **d** Plot of  $\ln(\alpha)$  versus photon energy of grown 2,2',4,4'-tetrahydroxybenzophenone single crystal. **e** Plot of skin depth versus photon energy of grown 2,2',4,4'-tetrahydroxybenzophenone single crystal

**Table 3** Optical parameters of 2,2',4,4'-tetrahydroxybenzophenone single crystal

Optical parameters	Calculated values
Optical band gap ( $E_g$ )	2.5 eV
Urbach energy ( $E_U$ )	0.182 eV
Steepness parameter ( $\alpha$ )	0.129
Electron–phonon interaction ( $E_{e-p}$ )	5.1679

other decomposition products [34]. The positive value of Gibb's free energy indicates that the decomposition of the grown crystal is non-spontaneous.

### 3.5 Dielectric studies

The dielectric properties are the fundamental studies of solids. The frequency dependence of these properties gives excellent insight into material applications. Electro-optic materials remain expanding for many applications, such as electro-optical modulators, where electric fields are applied to such crystals to modulate polarization. They are correlated with

the dielectric properties of the crystals [35]. The defect-free, good, quality transparent crystals were used for the dielectric studies. The cut and polished crystals were coated with perfect graphite on both sides were used for the dielectric measurements. The grown 2,2',4,4'-tetrahydroxybenzophenone single crystal dielectric measurements were carried out by an Agilent 4284A LCR meter with a conventional parallel plate capacitor method [36–39]. The capacitance ( $C_{crys}$ ) and dielectric loss ( $\tan\delta$ ) were analyzed in the temperature range from 333 to 423 K versus the frequency range 100 Hz to 1 MHz. The dielectric constant value was calculated by using the relation [40, 41]

$$\epsilon_r = \left( \frac{A_{air}}{A_{crys}} \right) \left( \frac{C_{crys} - C_{air} \left( 1 - \frac{A_{crys}}{A_{air}} \right)}{C_{air}} \right) \quad (15)$$

In the above relation,  $A_{crys}$  represent the area of the crystal,  $A_{air}$  is the area of the electrode,  $C_{crys}$  is the capacitance of the crystal, and  $C_{air}$  is the capacitance of the air of the same dimension as the crystal. The AC conductivity is calculated by using the relation,

$$\sigma_{ac} = \epsilon_0 \epsilon_r \omega \tan\delta \quad (16)$$

where  $\epsilon_0$  is the permittivity of free space,  $\epsilon_r$  is the dielectric constant,  $\omega$  is the angular frequency ( $\omega = 2\pi f$ , where  $f$  is the ac frequency),  $\tan\delta$  is the dielectric loss, and  $\sigma_{ac}$  is the ac conductivity. The dielectric constants versus temperature at different frequencies are shown in Fig. 8a. The degree of polarization and the charge displacement in the crystal determine the magnitude of the dielectric constant. The absence of space charge polarization

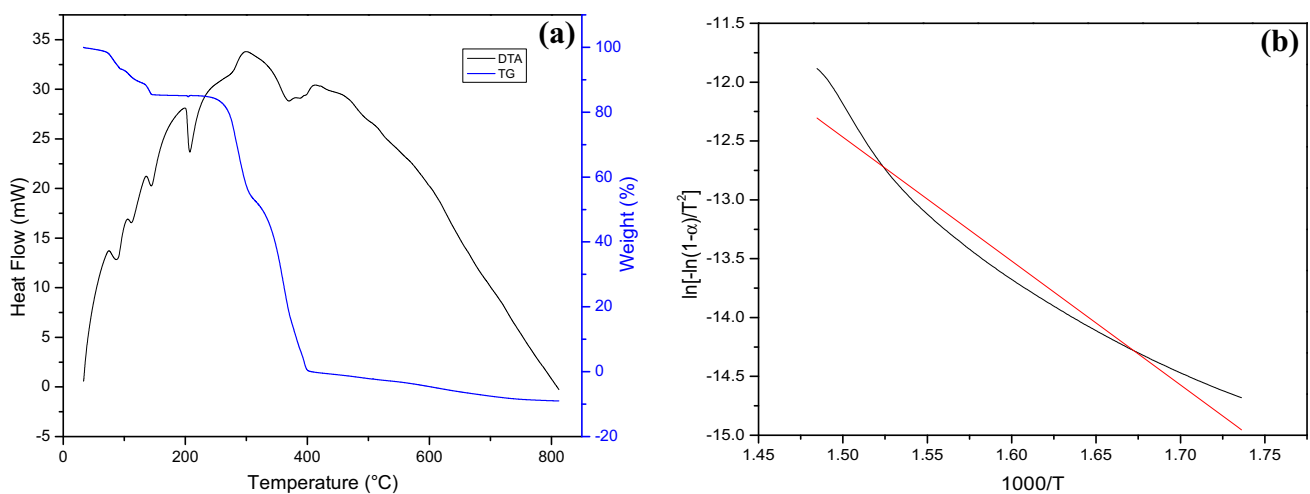


**Fig. 7** **a** TG/DTA graph of grown 2,2',4,4'-tetrahydroxybenzophenone. **b** Coats Redfern plot for 2,2',4,4'-tetrahydroxybenzophenone



**Table 4** Kinetic and thermodynamic parameters of 2,2',4,4'-tetrahydroxybenzophenone

Parameters	Calculated values
Activation energy ( $E_a$ ) kJ mol <sup>-1</sup>	87.57
Frequency factor ( $A$ ) s <sup>-1</sup>	1.39E + 6
Entropy ( $\Delta S^*$ ) J K <sup>-1</sup> mol <sup>-1</sup>	- 130.235
Enthalpy ( $\Delta H^*$ ) kJ mol <sup>-1</sup>	84.041
Gibb's free energy ( $\Delta G^*$ ) k J mol <sup>-1</sup>	139.39

near the grain boundary is attributed to decreased dielectric constants at higher frequencies. At low frequencies, the ionic, electronic, orientation, and space charge polarizations occur. The plot of dielectric loss (tanδ) versus temperature with different frequencies is shown in Fig. 8b. The low dielectric loss at high frequencies can be used for NLO applications. The variation of ac electrical conductivity with temperature is shown in Fig. 8c. Low dielectric constant materials use the least power and have a shorter RC delay, making them ideal for engineering microelectronics, electro-optic modulators, THz wave generators, optoelectronics, and photonic devices. The activation energy is calculated using the Arrhenius equation [29, 30]

$$\sigma_{ac} = \sigma_0 \exp\left(\frac{-E_a}{kT}\right) \tag{17}$$

where  $\sigma_{ac}$  is the electrical conductivity,  $\sigma_0$  is the pre-exponential parameter,  $E_a$  is the activation energy,  $T$  is the absolute temperature and  $k$  is Boltzmann's constant. Connecting the Arrhenius plot between  $\ln(\sigma_{ac})$  and  $1000/T$  is shown in Fig. 8d. It can be evaluated by using the formula [30, 33].

$$E_a = -k \times slope \tag{18}$$

The activation energy of 2,2',4,4'-tetrahydroxybenzophenone single crystal is calculated for various frequencies 100 Hz, 1 kHz, 10 kHz, 100 kHz, and 1 MHz. The calculated values are found to be 0.155, 0.122, 0.107, 0.086, and 0.0798 eV, respectively. The results show that the activation energy decreases with an increase in frequency, which may be due to an increase in field frequency, which is responsible for the electronic transition between the confined states. The grown single crystal dielectric constant value is used to find the electronic polarizability. The

high-frequency dielectric constant explicitly depends on the valence electron plasma energy, the Penn gap, and Fermi energy. The valence electron plasma energy is [42–46].

$$\hbar\omega_p = 28.8 \left(\frac{Z\rho}{M}\right)^{1/2} \tag{19}$$

The above relation gives the total number of valence electrons as  $Z$ , its density as  $\rho$ , and the molecular weight of the 2,2',4,4'-tetrahydroxybenzophenone as  $M$ . The Fermi energy is calculated by using the relation,

$$E_F = 0.2948(\hbar\omega_p)^{4/3} \tag{20}$$

By substituting the dielectric constant with the Plasma energy, the Penn gap is determined using the relation

$$E_P = \frac{(\hbar\omega_p)}{(\epsilon_r - 1)^{1/2}} \tag{21}$$

The polarizability ( $\alpha$ ) is obtained from,

$$\alpha = \left(\frac{(\hbar\omega_p)^2 S_0}{(\hbar\omega_p)^2 S_0 + 3E_P^2}\right) \times \frac{M}{\rho} \times 0.396 \times 10^{-24} \text{cm}^3, \tag{22}$$

where the Penn gap ( $E_P$ ) and the constant  $S_0$  are calculated by using the relation

$$S_0 = 1 - \left(\frac{E_P}{4E_F}\right) + \frac{1}{3} \left(\frac{E_P}{4E_F}\right)^2 \tag{23}$$

Using the Clausius–Mossotti equation, the value of  $\alpha$  is obtained by,

$$\alpha = \left(\frac{3M}{4\pi N_a \rho}\right) \left(\frac{\epsilon_r - 1}{\epsilon_r + 2}\right), \tag{24}$$

where the Avogadro Number is  $N_a$  ( $6.023 \times 10^{-23}$ ). The Penn gap, Fermi energy, and electronic polarizability are obtained from the valence electron plasma energy and the Clausius–Mossotti equation is shown in Table 5.

### 3.6 Nonlinear optical studies

The nonlinear properties of the grown 2,2',4,4'-tetrahydroxybenzophenone single crystal was analyzed by an effective Z-scan technique. The setup without an aperture is an open-aperture Z-scan technique. The Q-switched Nd:YAG laser with a

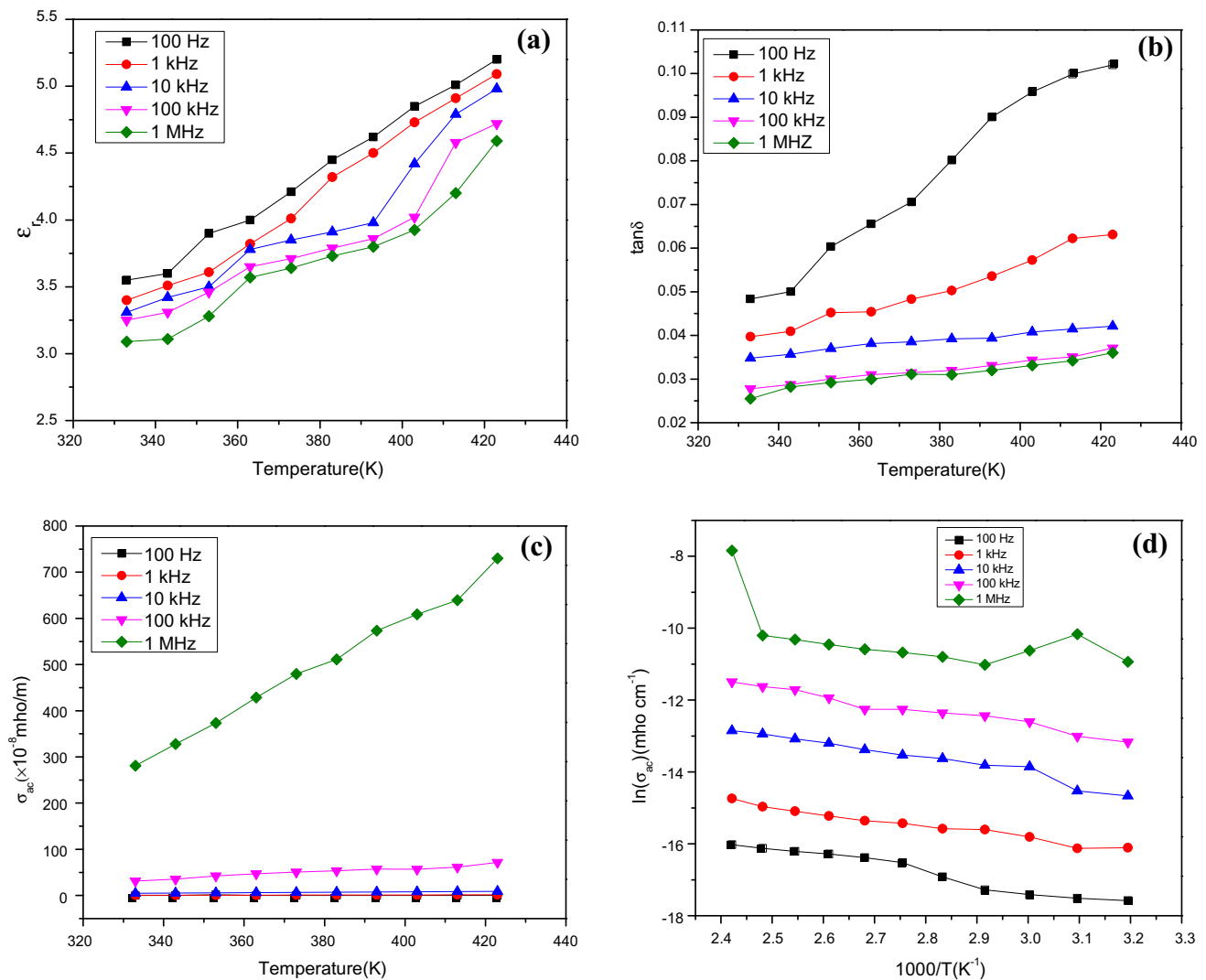


**Fig. 8** **a** Plot of dielectric constant variation of 2,2',4,4'-tetrahydroxybenzophenone. **b** Plot of dielectric loss variation of 2,2',4,4'-tetrahydroxybenzophenone. **c** Plot of Ac conductivity of

grown 2,2',4,4'-tetrahydroxybenzophenone. **d** Variation of activation energy of grown 2,2',4,4'-tetrahydroxybenzophenone single crystal

wavelength of 532 nm, a pulse energy of 100  $\mu\text{J}$ , and a pulse rate of 9 ns was used for the analysis. Here, the laser beam was focused using a plano-convex lens with a focal length of 15 cm. The laser beam was propagated along the Z-axis. The sample was taken in a 1 mm cuvette, and it was mounted on a stepper motor controlled linear translational stage between the lens and the focal point. The transmitted intensity was measured at the different positions by moving the sample along the Z-axis away from the focal point. The schematic diagram of the open-aperture Z-scan technique is shown in Fig. 9a. Using the obtained data; the graph was plotted between the position and normalized transmittance [47–50]. The

**Table 5** Electrical properties of 2,2',4,4'-tetrahydroxybenzophenone crystal

Parameters	Calculated values
Plasma energy ( $\hbar\omega_p$ )	18.511 eV
Fermi energy ( $E_F$ )	14.43 eV
Penn gap ( $E_P$ )	5.71 eV
Electronic polarizability ( $\alpha$ )	
Using Penn gap	$5.813 \times 10^{-23} \text{ cm}^3$
Using Clausius Mossotti relation	$5.971 \times 10^{-23} \text{ cm}^3$

plot shows a valley-like pattern with a maximum absorption intensity at the focus ( $Z = 0$ ). It

demonstrates that the 2,2',4,4'-tetrahydroxybenzophenone single crystal exhibits reverse saturated absorption. So, the grown crystal can be used for laser safety devices. The obtained Z-scan data were numerically connected with the nonlinear transmission equation given by Sheik-Bahae,

$$T = \left( \frac{1}{\sqrt{\pi}q_0(z,0)} \right) \int_{-\infty}^{\infty} \ln [1 + q_0(z,0)e^{-\tau^2}] d\tau, \quad (25)$$

where  $T$  is the normalized transmittance of the given sample and its pulse width is  $\tau$ .

$$q_0(z,0) = \frac{\beta I_0 L_{eff}}{\left(1 + \frac{z^2}{z_0^2}\right)}, \quad (26)$$

where  $\beta$  is the effective nonlinear absorption coefficient and  $I_0$  is the laser beam intensity at the focal point. The effective thickness of the sample is calculated using the formula

$$L_{eff} = \left( \frac{1 - e^{(-\alpha l)}}{\alpha} \right) \quad (27)$$

Let the linear absorption coefficient is  $\alpha$ , and the thickness of the sample cell is  $l$ . The Rayleigh length  $Z_0$  is given by,

$$Z_0 = \frac{\pi \omega_0^2}{\lambda} \quad (28)$$

The theoretical plots (solid line) match well with the experimental fits (solid circle) for two-photon absorption. It was shown in Fig. 9b. The estimated two-photon absorption coefficient value is  $1.25 \times 10^{-10} \text{ m W}^{-1}$ .

### 3.7 Optical limiting threshold

The optical limiting threshold measurements can be used to determine the critical power of the laser beam at which nonlinearity begins to impact the transmission. From the open-aperture Z-scan data, the optical limiting values were evaluated. The curve was

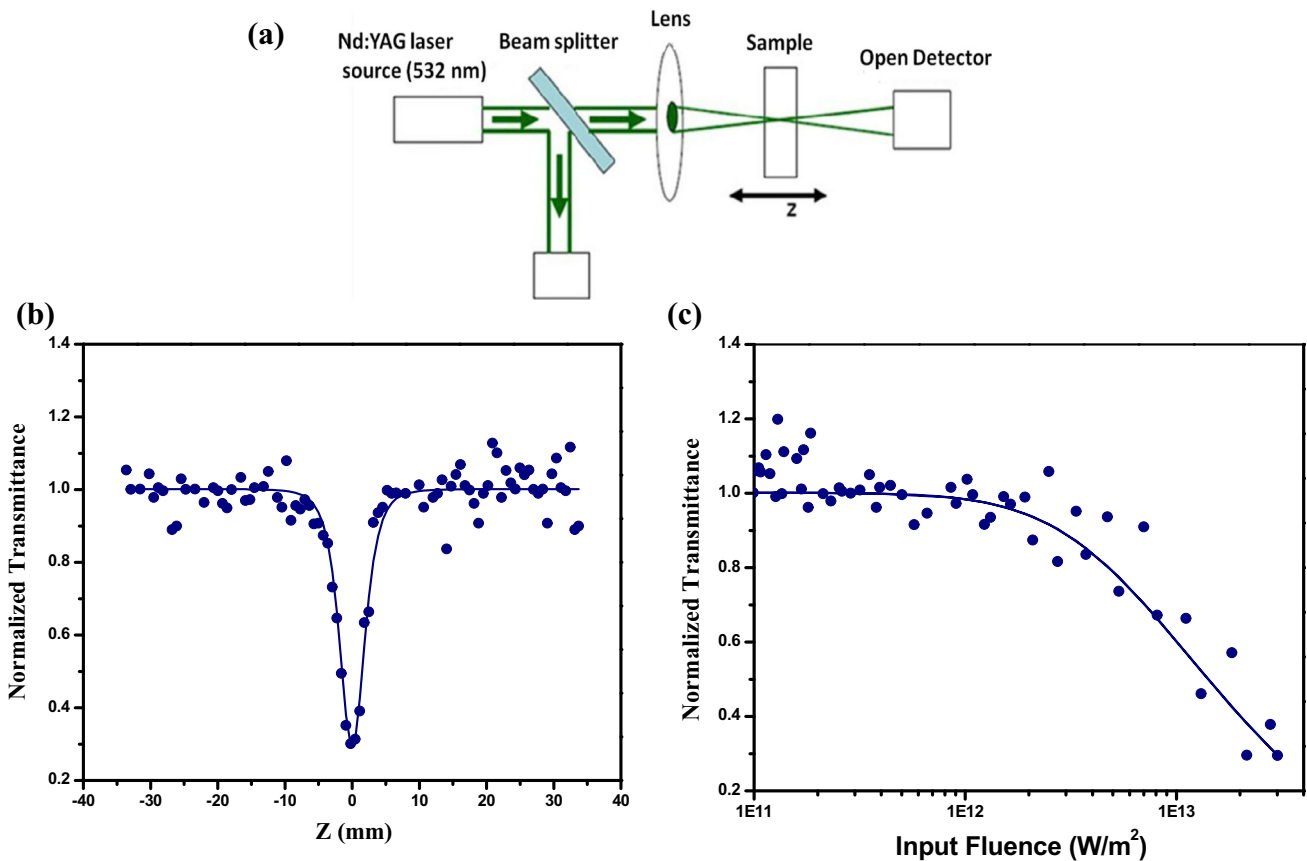


**Fig. 9** a Schematic diagram of open-aperture Z-scan technique. b Open-aperture Z-scan pattern of 2,2',4,4'-tetrahydroxybenzophenone. c Optical limiting curve of 2,2',4,4'-tetrahydroxybenzophenone

**Table 6** Estimated NLO coefficients of 2,2',4,4'-tetrahydroxybenzophenone

NLO Coefficients	Values
Saturation intensity, $I_s$	$30 \times 10^{11} \text{ W m}^{-2}$
Nonlinear absorption coefficient, $\beta$	$1.25 \times 10^{-10} \text{ m W}^{-1}$
Onset optical limiting threshold	$1.76 \times 10^{12} \text{ W m}^{-2}$

plotted between the normalized transmittance and input intensity ( $\text{W m}^{-2}$ ). The position-dependent fluence equation [51–53]

$$F(z) = 4\sqrt{\ln 2} \left( \frac{E_{in}}{\pi^{3/2} \omega(z)^2} \right), \quad (29)$$

where  $F(z)$  is the fluence,  $E_{in}$  is the incident laser energy. The graph shows the nonlinear pattern of the material, in which the output transmittance changes nonlinearly with input fluence. The nonlinearity input where the deviation begins is known as the onset optical limiting threshold. Thus, the grown 2,2',4,4'-tetrahydroxybenzophenone single crystal can work as an optical limiter; it can block the high intensity and transmit the low intensity. The experimental optical limiting threshold value is  $1.76 \times 10^{12} \text{ W m}^{-2}$ , and the graph between normalized transmittance and input fluence is shown in Fig. 9c. The grown 2,2',4,4'-tetrahydroxybenzophenone single crystal may be used as a safeguard for optical components from high intense laser. The calculated NLO coefficients are shown in Table 6.

## 4 Conclusion

The organic 2,2',4,4'-tetrahydroxybenzophenone single crystal was grown by a slow evaporation technique using ethanol as the solvent. The XRD studies reveal that the grown crystal belongs to a monoclinic crystal system with centrosymmetric space group C2/c. The functional groups present in the grown 2,2',4,4'-tetrahydroxybenzophenone crystal was verified using FTIR and FT-Raman analyses. In UV-Vis, studies show that the grown crystal cut-off wavelength was observed near 401 nm, and the calculated band gap is 2.5 eV which shows the grown crystal has photonic and optical applications. The grown crystal

melting and decomposition points are confirmed using TG/DTA analyses. The kinetic and thermodynamic parameters such as order of reaction, activation energy, entropy, enthalpy, and Gibbs free energy were calculated from the TGA data. The dielectric property of the grown crystal was observed using the conventional parallel plate capacitor method, and the electrical parameters such as plasma energy, Penn gap, Fermi energy, and polarizability were calculated. The open-aperture Z-scan studies reveal that the grown 2,2',4,4'-tetrahydroxybenzophenone exhibits reverse saturable absorption owing to two-photon absorption. The optical limiting threshold studies show that the grown 2,2',4,4'-tetrahydroxybenzophenone single crystal may be used as a safeguard for optical components from the high intense laser.

## Acknowledgements

This work was supported by the University Grants Commission (UGC), South Eastern Regional Office (SERO), Government of India, under the grant of Minor Research Project UGC Reference No: F. MRP-7005/16 (SERO/UGC) Link No: 7005, is hereby gratefully acknowledged.

## Author contributions

All authors contributed to the study's conception and design. Material preparation, data collection, and analysis were performed by all authors. All authors read and approved the final manuscript.

## Funding

This study was funded by University Grants Commission—South Eastern Regional Office, 7005/16, T. Suthan.

## Data availability

All data generated or analyzed during this study are included in this manuscript.

## Declarations

**Competing interest** The authors declare that they have no conflict of interest.

## References

- V. Usharani, J. Natarajan, M. Judes, P. Arivanandhan, S. Anandan, *Optik* **127**, 5887–5893 (2016)
- L. Wang, C. Liu, S. Shen, Xu. Mingzhen, X. Liu, *Adv. Ind. Eng. Polym. Res.* **3**, 138–148 (2020)
- B.D. Hatton, K. Landskron, W.J. Hunks, M.R. Bennett, D. Shukaris, D.D. Perovic, G.A. Ozin, *Mater. Today* **9**, 22–31 (2006)
- T. Suthan, N.P. Rajesh, C.K. Mahadevan, G. Bhagavan-narayana, *Spectrochim. Acta Part A* **78**, 771–776 (2011)
- T. Suthan, N.P. Rajesh, C.K. Mahadevan, K. Senthil Kumar, G. Bhagavannarayana, *Spectrochim. Acta Part A* **79**, 1443–1448 (2011)
- S.R. Yousefi, M. Ghanbari, O. Amiri, Z. Marzhooseyni, P. Mehdizadeh, M. Hajizadeh-Oghaz, M. Salavati-Niasari, *J. Am. Ceram. Soc.* **104**, 2952–2965 (2021)
- S.R. Yousefi, H.A. Alshamsi, O. Amiri, M. Salavati-Niasari, *J. Mol. Liq.* **337**, 116405 (2021)
- M.A. Mahdi, S.R. Yousefi, L.S. Jasim, M. Salavati-Niasari, *Int. J. Hydrog. Energy* **47**, 14319–14330 (2022)
- T. Suthan, P.V. Dhanaraj, N.P. Rajesh, C.K. Mahadevan, G. Bhagavannarayana, *Cryst. Eng. Comm* **13**, 4018–4024 (2011)
- S. Usharani, J. Judes, V. Natarajan, M. Arivanandhan, P. Anandan, D.A. Vorontsov, M.O. Marychev, *Opt. Mater.* **100**, 109603 (2020)
- V. Natarajan, M. Arivanandhan, P. Anandan, K. Sankaranarayanan, G. Ravi, Y. Inatomi, Y. Hayakawa, *Mater. Chem. Phys.* **144**, 402–408 (2014)
- E.O. Schlemper, *Acta Cryst.* **B38**, 554–559 (1982)
- J.-P. AntonioGarcia-Jimenez, P. AntonioGarcia-Ruiz, J.-L. JoseBerna, F.-C. JoseTudela, *Int. J. Biol. Macromol.* **98**, 622–629 (2017)
- E. Smith, G. Dent, *Modern Raman spectroscopy—a practical approach* (John Wiley & Sons Ltd, England, 2005)
- G. Socrates, *Infrared and Raman characteristic group frequencies: tables and charts* (John Wiley and sons Ltd, Chichester, 2001)
- J. Coates, *Interpretation of infrared spectra—a practical approach* (John Wiley & Sons Ltd, Chichester, 2000)
- V. Krishnakumar, S. Muthunatesan, G. Keresztury, T. Sundius, *Spectrochim. Acta Part A* **62**, 1081–1088 (2005)
- C.N. Banwell, E.M. McCash, *Fundamentals of molecular spectroscopy*, 4th edn. (Tata McGraw-Hill, New Delhi, 1994)
- R.P. Jebin, T. Suthan, T.R. Anitha, N.P. Rajesh, G. Vinitha, *J. Mater. Sci.: Mater. Electron.* **32**, 3232–3246 (2021)
- B.S. Arun Sasi, R.P. Jebin, T. Suthan, C. James, *J. Mol. Struct.* **1146**, 797–807 (2017)
- A.J.A. Pragasam, M. Divya, A.V. Pani Vignesh, G. Vinitha, P. Malliga, *Opt. Laser Technol.* **107**, 428–434 (2018)
- S.R. Yousefi, O. Amiri, M. Salavati-Niasari, *Ultrason. Sono Chem.* **58**, 104619 (2019)
- A. Rathika, G. Raman, *Mater. Res. Innov.* **19**, 3 (2015)
- G. Rajasekar, M.K. Dhatchaiyini, P. Rekha, S. Sudhahar, G. Vinitha, A. Bhaskaran, *J. Mater. Sci.: Mater. Electron.* **31**, 18732–18744 (2020)
- K. Senthil, S. Kalainathan, A. Ruban Kumar, P.G. Aravindan, *RSC Adv.* **4**, 56112–56127 (2014)
- T. Arumanayagam, P. Murugakoothan, *J. Miner. Mater. Charact. Eng.* **10**, 1225–1231 (2011)
- P.P. Abirami Priya, T. Suthan, S.A. Thambi Raja, V. Bena Jothy, *J. Mater. Sci.: Mater. Electron.* **33**, 14214–14227 (2022)
- K. Gayathri, P. Krishnan, P.R. Rajkumar, G. Anbalagan, *Bull. Mater. Sci.* **37**, 1589–1595 (2014)
- S. Prince, T. Suthan, C. Gnanasambandam, N.P. Rajesh, G. Vinitha, *J. Mater. Sci.: Mater. Electron.* **33**, 5909–5923 (2022)
- S. Prince, T. Suthan, C. Gnanasambandam, *J. Electron. Mater.* **51**, 1639–1652 (2022)
- C. Li, K. Suzuki, *J. Therm. Anal. Calorim.* **98**, 261–266 (2009)
- S. Gul, A.H. AliShah, S. Bilal, *J. Sci. Innov. Res.* **2**(3), 673–684 (2013)
- S. Prince, T. Suthan, S. Goma, C. Gnanasambandam, N.P. Rajesh, *J. Mater. Sci.: Mater. Electron.* **34**, 165 (2023)
- B.K. Singh, J. Chandra, H.K. Rajor, *Int. J. Appl. Chem.* **13**, 235–253 (2017)
- J. Balaji, P. Srinivasan, S. Prabu, M. George, D. Sajan, *J. Mol. Struct.* **1207**, 127750 (2020)
- T. Suthan, N.P. Rajesh, P.V. Dhanaraj, C.K. Mahadevan, *Spectrochim. Acta Part A* **75**, 69–73 (2010)
- R.B. Kulkarni, S.S. Hussaini, M.D. Shirsat, *Mater. Today: Proc.* **23**, 423–429 (2020)
- P. Balamurugaraj, S. Suresh, P. Koteeswari, P. Mani, *J. Mater. Phys. Chem.* **1**, 4–8 (2013)
- T. Suthan, N.P. Rajesh, *J. Cryst. Growth* **312**, 3156–3160 (2010)
- T. Suthan, N.P. Rajesh, C.K. Mahadevan, G. Bhagavan-narayana, *Mater. Chem. Phys.* **129**, 433–438 (2011)
- T. Suthan, P.V. Dhanaraj, N.P. Rajesh, *Spectrochim. Acta Part A* **87**, 194–198 (2012)
- S. Kalyanaraman, P.M. Shajinshinu, S. Vijayalakshmi, *Phys. B* **482**, 38–42 (2016)

43. S.S. Bala Solanki, N.P. Rajesh, T. Suthan, J. Mater. Sci.: Mater. Electron. **32**, 1808–1817 (2021)
44. S. Kalyanaraman, P.M. Shajinshinu, S. Vijayalakshmi, J. Phys. Chem. Solids **86**, 108–113 (2015)
45. B. Aneebea, S.V. Ashvin Santhia, S. Vinu, R. Sheela Christy, J. Mater. Sci.: Mater. Electron. **32**, 16961–16969 (2021)
46. S.S. Bala Solanki, N.P. Rajesh, T. Suthan, Opt. Laser Technol. **103**, 163–169 (2018)
47. C. Babeela, N.K. Siji Narendran, M. Pannipara, A.G. Al-Sehemi, T.C. Sabari Girisun, Mater. Chem. Phys. **237**, 121827 (2019)
48. K. Thukral, N. Vijayan, D. Haranath, K.K. Maurya, J. Philip, V.J. Ayaramakrishnan, Arab. J. Chem. **12**, 3193–3201 (2019)
49. M. Thangaraj, G. Vinitha, T.C. SabariGirisun, P. Anandan, G. Ravi, Opt. Laser Technol. **73**, 130–134 (2015)
50. M.L. Lima Rose, T. Suthan, C. Gnanasambandam, T.C. Sabari Girisun, J. Mater. Sci.: Mater. Electron. **34**, 884 (2023)
51. M. Saravanan, T.C. Sabari Girisun, Mater. Chem. Phys. **160**, 413–419 (2015)
52. A. Pramothkumar, N. Senthilkumar, R. MaryJenila, M. Durairaj, T.C. SabariGirisun, I.V. Potheher, J. Alloys Compd. **878**, 160332 (2021)
53. M. Monisha, N. Priyadarshani, M. Durairaj, T.C. Sabari Girisun, Opt. Mater. **101**, 109775 (2020)

**Publisher's Note** Springer Nature remains neutral with regard to jurisdictional claims in published maps and institutional affiliations.

Springer Nature or its licensor (e.g. a society or other partner) holds exclusive rights to this article under a publishing agreement with the author(s) or other rightsholder(s); author self-archiving of the accepted manuscript version of this article is solely governed by the terms of such publishing agreement and applicable law.